Electrochemical Applications

1/97

Advances in electrochemical applications of impedance spectroscopy
Issued and © by ZAHNER-elektrik GmbH & Co. KG, August 1997

# *Multiple phases ...*

... of matter in an electrochemical system may be arranged more discrete or more percolated. This different states of homogeneity have influence on most properties, which are meaningful in technical applications of such systems. In issue 1/95 of this magazine we discussed a special case of inhomogeneity: Surface layers with conductance gradients perpendicular to their surface are mainly of interest in the fields of corrosion, passivation and coating. In this issue we will continue with the discussion of non-homogeneous systems - but with that kind of inhomogeneity which is characterizing porous systems.

It is a common way to construct electrochemical cells by means of porous electrodes, if one is forced to increase the maximum current density under limited spatial conditions. The trick is to increase the electrochemically active area at constant geometrical dimensions.

Porous systems are of interest for many fields, for instance for sensor technology. This issue of **ElApps** will focus on systems, designed for power generation like batteries or fuel cells. At a smooth electrode, the electro-active two-phase-boundary between the ion-conducting and the electron-conducting phase is planar. The transition from a smooth electrode to a porous one may be understood as a folding-up in the third dimension. One characteristic of the so built pores is, that areas of active surface in different depths generally have different distances to the equipotential planes represented by sections through the bulk phases. In practice this causes a different coupling to the current collectors and to the transport paths for products and educts.

A further complication arises, if products or educts respectively are in the gas phase, as it is the case in fuel cells. In the meaning of the following articles, such three-phase-boundary systems shall be characterized with the term "porous" in the same way, if a porous fold up of the ion-electron-conduction interphase (double layer) exists. Since 1961 [1] such systems were treated theoretically. Generally, the authors do not assume an inhomogeneous behavior of the electrodes in lateral direction to the surface. Although specific problems with lateral non-uniform current densities are of practical relevance (for instance at a high gas throughput in fuel cells), they cannot be treated here, in contrast to the behavior perpendicular to the geometric surface (or in the direction of the pore orientation).

Our first article (author H. Göhr) reports of systems, which are homogeneous too with respect to the double layer electrochemical activity in that pore direction. His term "*homogeneous pore system*" characterizes a porous electrode, which is not only homogeneous (invariant on periodic translations) in the direction of the two dimensions of the geometric surface, but also along the pore depth. It must be mentioned, that this kind of uniform pore activity does not restrict the model on cases, where a uniform direct current distribution must exist. As a consequence, this model could be successfully used in the work reported by F. Richter in the second article. Here the *homogeneous pore model* was applied to the development and quality control of high temperature fuel cells. In particular the less problematic zero current case and the case of current sourceing up to a density of about 0.3 A/cm$^2$ (geometric area) is discussed.

In the third contribution W. Paasch introduces a model of a "*system of inhomogeneous pores*", which is no longer based on the assumption of uniform electrochemical activity along the pore axis. One should expect such inhomogeneous pore properties for instance, if high current densities will shift the bias of the charge transfer to the exponential branch of the Butler-Volmer-curve, or if rate determining diffusion processes in the pores occur.

Generally, coming from a more simple description to the models of homogeneous and finally inhomogeneous pore systems, the number of characteristic model parameters increases. On the other hand, the experimental impedance data become less expressive when moving from smooth electrodes to porous ones. The difficulties coming up from this contrary situation are obvious. But the work of F. Richter demonstrates, that under certain conditions otherwise inaccessible information will be obtained by means of such models. (CAS)

[1] K.J. Euler: Die Verteilung der Stromdichte über die Dicke von ebenen porösen Gas-Elektroden in elektrochemischen Stromquellen, Ann. Physik. 7. Folge, Bd. 26

# *Impedance Modelling of Porous Electrodes*

**by H. Göhr**
Erlangen

In the discussed model there are 5 impedances that contribute to the sum impedance of a porous electrode. These are $\boldsymbol{Z}_q$ of the interior interface area $A_i$ of the pore system, $\boldsymbol{Z}_p$ of the pores filled with electrolyte, $\boldsymbol{Z}_s$ of the porous layer as well as $\boldsymbol{Z}_e$ and $\boldsymbol{Z}_m$ at the outer contact areas $\boldsymbol{A}_e$ electrolyte/layer material and $\boldsymbol{A}_m$ pores/metallic body (fig.1 & 3).

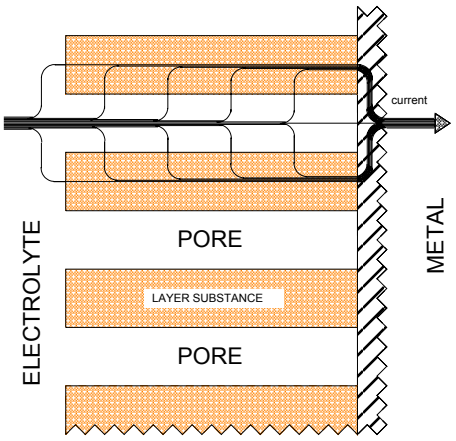


Fig.1: Skeleton sketch of a porous electrode system and flow of alternating current.

If $\boldsymbol{A}_i$ is sufficiently bigger than $\boldsymbol{A}_e$ and/or $\boldsymbol{A}_m$, $\boldsymbol{Z}_e$ or $\boldsymbol{Z}_m$ respectively can be dropped ($\boldsymbol{Z}_e \to \infty$ or $\boldsymbol{Z}_m \to \infty$). By dissecting the pore system (thickness $\delta$) into n slices of the thickness d = $\delta$/n (fig.2) with the impedances $\boldsymbol{z}_{qi}$, $\boldsymbol{z}_{pi}$, $\boldsymbol{z}_{si}$ (i = 1, 2, ... n) occurring there, $\boldsymbol{Z}_q$ results in the reciprocal of the sum of the admittances $\boldsymbol{z}_{qi}^{-1}$ and $\boldsymbol{Z}_p$ and $\boldsymbol{Z}_s$ in the sum of $\boldsymbol{z}_{pi}$ or $\boldsymbol{z}_{si}$ respectively. If the pore system is homogeneous so that $\boldsymbol{z}_{qi} = \boldsymbol{z}_q$, $\boldsymbol{z}_{pi} = \boldsymbol{z}_p$ and $\boldsymbol{z}_{si} = \boldsymbol{z}_s$ correspond in all slices, for $n \to \infty$ one gets an analytical expression as a link of all 5 impedances. To achieve a clear description auxiliary complex variables are defined[1]:

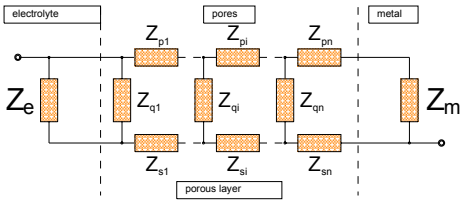


$$1/Z_q = 1/z_{q1} + 1/z_{q2} + \ldots + 1/z_{qn}$$
$$Z_p = z_{p1} + z_{p2} + \ldots + z_{pn}$$
$$Z_s = z_{s1} + z_{s2} + \ldots + z_{sn}$$

Fig.2: Sectioning of a pore system of thickness $\delta$ into n slices no i=1,..., n (thickness d=$\delta$/n) and connections of the impedances $z_{qi}$, $z_{pi}$, $z_{si}$ within slice no i, and of $Z_e$ and $Z_m$.

$$\boldsymbol{Z}^* = \left[\left(\boldsymbol{Z}_p + \boldsymbol{Z}_s\right) \cdot \boldsymbol{Z}_q\right]^{1/2},$$
$$\boldsymbol{Z}\,\| = \boldsymbol{Z}_p \cdot \boldsymbol{Z}_s \,/\, \left(\boldsymbol{Z}_p + \boldsymbol{Z}_s\right),$$
$$\boldsymbol{q}_e = \boldsymbol{Z}^* \,/\, \boldsymbol{Z}_e\,,\ \boldsymbol{q}_m = \boldsymbol{Z}^* \,/\, \boldsymbol{Z}_m\,,$$
$$\boldsymbol{p} = \boldsymbol{Z}_p \,/\, \left(\boldsymbol{Z}_p + \boldsymbol{Z}_s\right),\ \boldsymbol{s} = \boldsymbol{Z}_s \,/\, \left(\boldsymbol{Z}_p + \boldsymbol{Z}_s\right),$$
$$\nu = \left[\left(\boldsymbol{Z}_p + \boldsymbol{Z}_s\right) / \boldsymbol{Z}_q\right]^{1/2},\ \boldsymbol{T} = \tanh(\nu)$$

The impedance of the homogeneous pore system then is:

$$\boldsymbol{Z} = \boldsymbol{Z}\,\| + \boldsymbol{Z}^* \cdot \frac{1 + 2\,\boldsymbol{ps}\left[\left(1 - \boldsymbol{T}^2\right)^{1/2} - 1\right] + \boldsymbol{T} \cdot \left(\boldsymbol{p}^2 \boldsymbol{q}_m + \boldsymbol{s}^2 \boldsymbol{q}_e\right)}{\boldsymbol{T} \cdot \left(1 + \boldsymbol{q}_e \cdot \boldsymbol{q}_m\right) + \boldsymbol{q}_e + \boldsymbol{q}_m}$$

In the case of inhomogenities no general valid expression could be found. Then only special cases could be discussed.

$\boldsymbol{Z}_q$ (as well as $\boldsymbol{Z}_e$ and $\boldsymbol{Z}_m$) corresponds to a parallel connection of a double layer impedance and a Faraday impedance, which besides a transfer resistance also provides diffusion and adsorption shares. $\boldsymbol{Z}_p$ and $\boldsymbol{Z}_s$ generally can be described as resistors. In the case of a metallic pore system mostly $\boldsymbol{Z}_p$ = 0. Then p = 0 and $\boldsymbol{Z}\,\|$ = 0. In regard to $\boldsymbol{Z}^*$ should be mentioned: In the case $\boldsymbol{Z}_p$ = R and $\boldsymbol{Z}_s$ = $R_s$ are resistors, the phase shift $\varphi$(f) of $\boldsymbol{Z}^*$ is exactly half of the one of $\boldsymbol{Z}_q$ because of the square root at each frequency[2].

Mainly special cases are of interest as in the general case so much parameters will be found, that one can determine these parameters only hardly without additional knowledge[3] by fitting the calculated with the measured impedance spectra.

**Special case 1:**

$$\boldsymbol{Z}_e = \boldsymbol{Z}_m \to \infty$$
$$\boldsymbol{Z} = \boldsymbol{Z}\,\| + \boldsymbol{Z}^* \cdot \frac{1 + 2\,\boldsymbol{ps}\left[\left(1 - \boldsymbol{T}^2\right)^{1/2} - 1\right]}{\boldsymbol{T}}$$

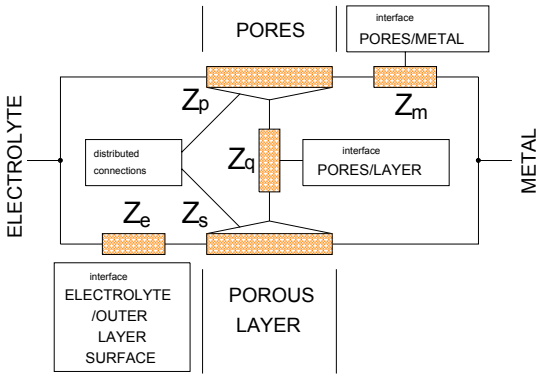


Fig.3: Equivalent circuit of a homogeneous pore system.

**Special case 2:**

$$\boldsymbol{Z_p = 0} \text{ or } \boldsymbol{Z_s} \ (\boldsymbol{p = 0} \text{ or } \boldsymbol{s = 0} \text{ resp } \boldsymbol{Z \parallel = 0})$$

$$\boldsymbol{Z} = \frac{1 + \boldsymbol{T} \cdot \boldsymbol{Z}^* / \boldsymbol{Z_e}}{\boldsymbol{T} / \boldsymbol{Z}^* \cdot \left[1 + \boldsymbol{Z}^{*2} / (\boldsymbol{Z_e} \cdot \boldsymbol{Z_m})\right] + 1 / \boldsymbol{Z_e} + 1 / \boldsymbol{Z_m}}$$

**Special case 3:**

$$\boldsymbol{Z_e = Z_m \to \infty} \text{ and } (\boldsymbol{Z_p = 0} \text{ or } \boldsymbol{Z_s = 0})$$

$$\boldsymbol{Z} = \frac{\left[\boldsymbol{Z_s} \cdot \boldsymbol{Z_q}\right]^{1/2}}{\tanh\left(\left[\boldsymbol{Z_s} / \boldsymbol{Z_q}\right]^{1/2}\right)} \quad \text{or}$$

$$\boldsymbol{Z} = \frac{\left[\boldsymbol{Z_p} \cdot \boldsymbol{Z_q}\right]^{1/2}}{\tanh\left(\left[\boldsymbol{Z_p} / \boldsymbol{Z_q}\right]^{1/2}\right)}$$

[1] The tanh for real arguments $-\infty<v<\infty$ is limited to the range of $-1<\tanh(v)<1$.

[2] This means that $Z^*$ corresponds to a Warburg impedance (with $\varphi=-45°$), if $Z_q=(j\omega C)^{-1}$ is capacitive.

[3] Especially the measurement or estimation of one or more impedances $Z_p$, $Z_s$, $Z_q$, $Z_e$, $Z_m$.

# *Impedance Measurements under High Current for Development and Quality Control of Solid Oxide Fuel Cells (SOFCs)*

**by Franz Richter**
Siemens AG, KWU, Erlangen, Germany

SOFCs with oxidion-conducting electrolytes have been developed for temperatures from 750°C to 1100°C with various designs. The planar variant, developed by the Siemens AG, contains stacks of single cells which are connected through metallic connectors.

A sketch is shown in figure 1. Usually, the gastight electrolyte consists of doped zirconia ($ZrO_2$), whereas anode and cathode consist of nickel-cermet and a mixture of doped lanthanum-anganite ($LaMnO_3$) and electrolyte material. The electrodes could be composed of several porous layers of a different composition. Figure 1 does not include all additional layers of materials which ensure the electronic contact to the stack or which act as a diffusion barrier.

It will only be possible to develop efficient fuel cells, if appropriate diagnosis procedures are available to check the quality of the whole cell and the quality of the single layers, for example for each individual electrode. The use of potential probes has been discussed [1] for the electric characterization of layers. This method is, however, not free of problems, as potential probes in realistic cells can only be fixed on the edge, which means fixing on a surface with a distorted electric field. Impedance measurements on complete, sufficiently small cells could be a solution for this.

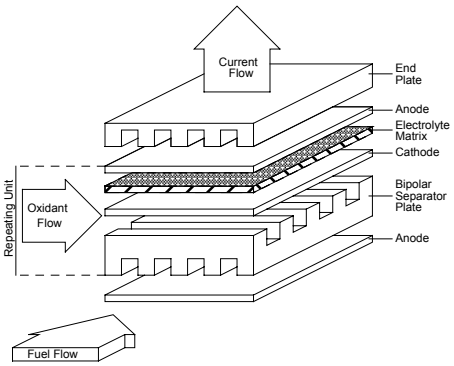


Fig.1: Planar arrangement of SOFC components.

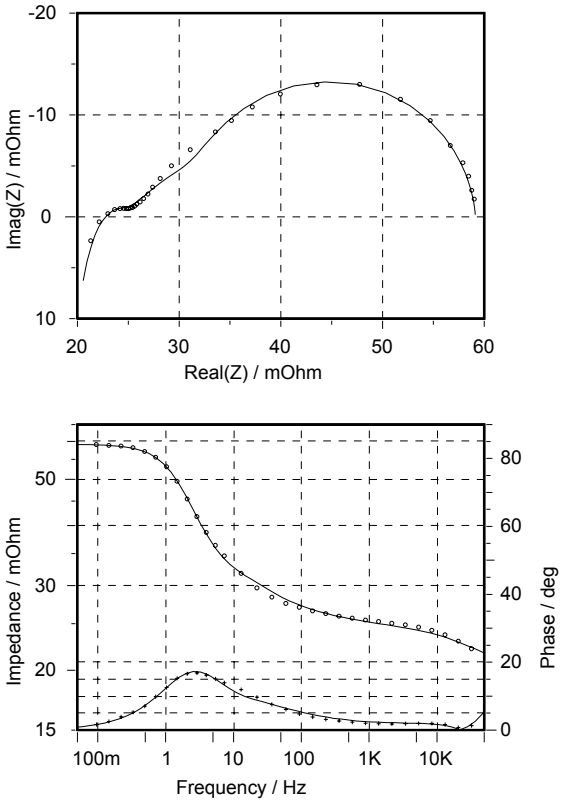


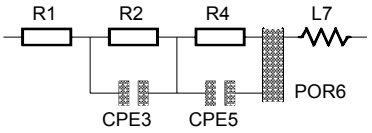


| N# | Value | Significance | Error/% |
|---|---|---|---|
| 1 | 18.04 mΩ | 0.83 | 2.25 |
| 2 | 6.46 mΩ | 0.24 | 4.31 |
| 3 | 1.517 mF<br>684 m | 0.10<br>82.73 | 18.73<br>0.01 |
| 4 | 27.94 mΩ | 0.47 | 0.53 |
| 5 | 2.273 F<br>952.1 m | 0.29<br>26.36 | 3.27<br>0.01 |
| 6 | 1<br>21.19 mΩ<br>0 Ohm | 0.17 | 10.67 |
| 7 | 13.06 nH | 13.42 | 0.06 |
| modulus impedance error: mean 0.2 %, max. 2.7 %<br>phase angle error: mean 0.1 deg, max. 1.5 deg | | | |

Tab. 1: Fit results of the system described in Fig.2

Fig. 2: Nyquist and Bode plots of the impedance spectra for a SOFC at 850°C and at rest potential of -0.92V. Fuel gas: $H_2$ with 50% humidity, oxidant: air, 30 l/h both. Circles: measured data, lines: modeled curves. The EC does not consider the $H_2O$ diffusion behavior at the anode.

The latest developments in the field of measuring techniques allow evaluations on cells with an internal resistance of 10 mΩ up to the high frequency end of 100 KHz. This corresponds to a maximum electrode area of about 4 times 4 $cm^2$. Stacks with all essential layers and typical channels for the gas supply of larger stacks can be verified in that kind of setup.

In principle, the electrical parameters of larger devices can be determined by analyzing the frequency response with the help of „equivalent circuits“: As a result of extended phase boundaries between electrodes and electrolyte material in the electrodes, these cell components show a negative imaginary part with approximately the same frequency-dependence as the one of a capacitance (double-layer capacitance). The Faraday impedance of the electrochemical charge transfer is connected in parallel. The Faraday impedance with a real part at low frequencies enables a flow of direct current through the cell down to $\omega \rightarrow 0$. This "shunting" is the reason why one can distinguish between the electrodes and the behavior of the bulk layers. Normally the other layers show a real response in the complex impedance plane with the share of the electrolyte resistance dominating.

Series connections of bulk resistances cannot be subdivided further, so that measurements in simplified systems with a reduced number of layers have to be used in order to determine the individual contributions.

An empirical equivalent circuit can be applied for the simulation of impedance spectra. Besides a series resistance and an inductivity, the equivalent circuit contains time constants of parallel R/C and R/CPE (CPE = *constant phase element*) combinations. The time constants due to anode and cathode respectively is insured by varying of the measurement conditions such as

- variation of the gas supply
- specific damage of anode or cathode
- measurements on so-called „symmetric cells“

The results have been very useful for the development of electrode/electrolyte units. On the one hand, a complete full area contact between electrodes and interconnector, which is necessary to achieve and to evaluate performance, could be proved with the help of the information about the series resistance. On the other hand, R out of R/C and R/CPE combinations directly results in the differential polarization resistances $R_p$ equal to R of the electrodes by means of:

$$\text{real part (CPE)} \rightarrow \infty \quad \text{for} \quad \omega \rightarrow 0 \qquad (1)$$

When looking at the structure of porous electrodes, which is active in three dimensions, it becomes clear that simple combinations of resistances and capacitances free from losses cannot precisely reflect the characteristics of electrodes. The reason for this is considerable electrochemical activity

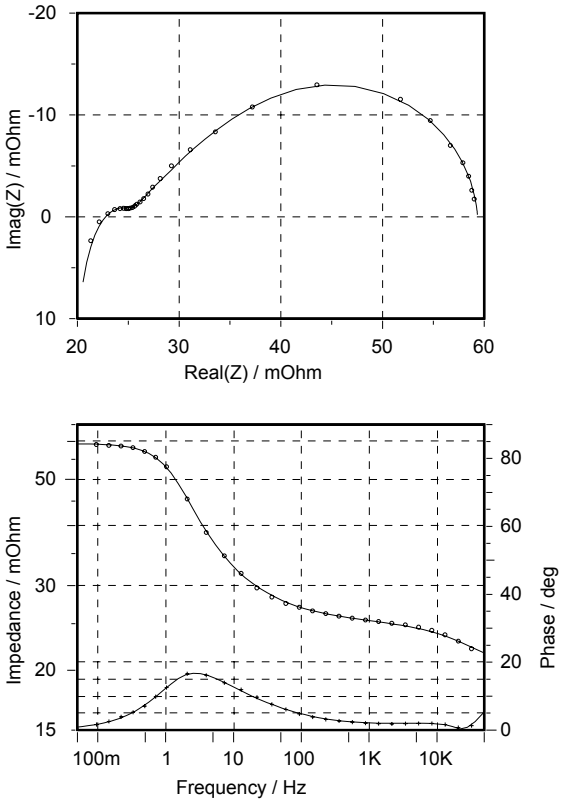


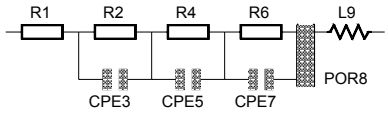


| N# | Value | Significance | Error/% |
|---|---|---|---|
| 1 | 18.21 mΩ | 0.84 | 2.25 |
| 2 | 6.731 mΩ | 0.25 | 2.09 |
| 3 | 1.656 mF<br>685.5 m | 0.11<br>51.80 | 18.06<br>0.01 |
| 4 | 4.207 mΩ | 0.08 | 9.61 |
| 5 | 4.268 F<br>1 | 0.06<br>3.61 | 11.69<br>0.34 |
| 6 | 25.81 mΩ | 0.43 | 0.94 |
| 7 | 2.733 F<br>953.5 m | 0.26<br>25.59 | 3.03<br>0.02 |
| 8 | 1<br>13.64 mΩ<br>0 Ohm | 0.12 | 6.20 |
| 9 | 13.28 nH | 8.23 | 0.06 |
| modulus impedance error: mean 0.1 %, max. 1.4 %<br>phase angle error: mean 0.0 deg, max. 0.6 deg | | | |

Tab 2: Fit results of the system described in Fig.3

Fig 3: Nyquist and Bode plots of the impedance spectra for a SOFC at 850°C and at rest potential of -0.92V. Fuel gas: $H_2$ with 50% humidity, oxidant: air, 30 l/h both. Circles: measured data, lines: modeled curves. The EC is extended by the elements R4 and CPE5. They represent the diffusion hindrance of $H_2O$ in $H_2$ at the anode.

within the electrodes, which follows from the desired enlargement of the triple phase boundary between electrolyte, electrode material and gas phase for the purpose of high current densities. The consequence of this spatial expansion is the coupling of active electrode areas to the electrolyte via ionic conductivity and to the metallic connector of the relevant electrode via electronic conductivity. In some cases, the equivalent circuit of a R/CPE combination therefore provides a useful approximation within a limited frequency range. There are, however, better models based on equivalent circuits, whose essential approach is the same in each of the following assumptions:

- the electrode be homogeneous in its area
- limitations regarding the conductivity are only considered in the direction of the thickness of the electrodes
- the electrochemical exchange of charge across the phase boundaries of electrolyte/electrode is treated as a bridge between the electronic and the ionic conductivity

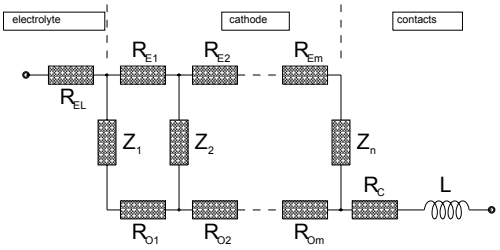


Fig. 4: Chain ladder model of a cathode.

Models and the related impedances have become known under names, such as ladder network, homogeneous pore system and transmission line model (TLM) [2,3,4]. Figure 4 shows the equivalent circuit of that kind of ladder network used on the cathode of a SOFC [5]. In the following, some examples of the impedance of cells within technically useable stacks and gastight-soldered housings are shown. The geometric electrode area is 16 $cm^2$. Figure 2 shows the cell impedance at rest potential. In the presented Bode and Nyquist diagrams, the marked points are those measuring points which have been selected as samples for the simulation. The streaked lines indicate the simulated impedance. The figure shows the applied equivalent circuit. The anode process was simulated by a R/CPE combination. (It could be proved that the high-frequency arc is assigned to the anode, in this case simulated by the parameters 2 and 3). This approximation, which has already been discussed earlier in this report, is precise enough, as the contribution of the anode to the overall polarization of the cell is low. The parameters 4,5 and 6 in figure 2 reflect the model of the ladder network for the cathode, with the ionic and electronic conductivity appearing as resistance values 21.19 mΩ and zero respectively; according to figure 4 (zero means a negligible small value).

These contributions have been verified and acknowledged during special measurements. According to the 2nd reference, the summarized polarization resistance of the cathode is:

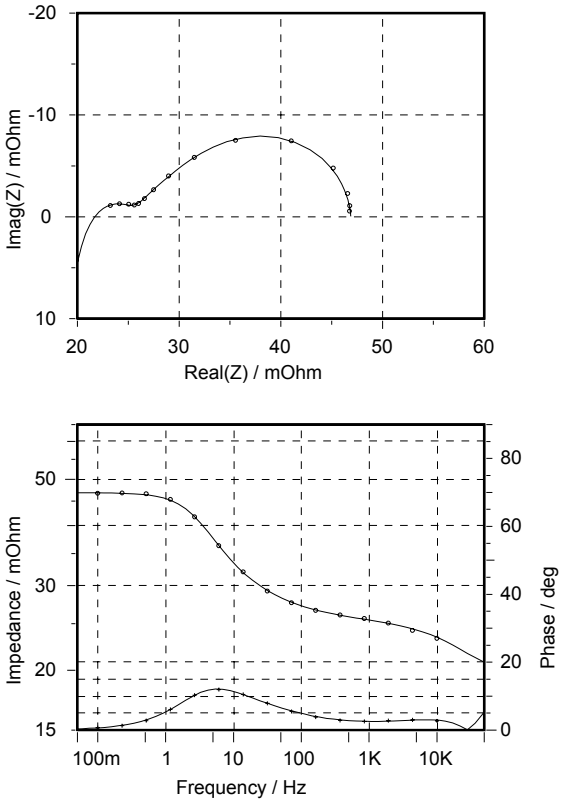


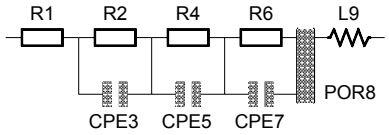


| N# | Value | Significance | Error/% |
|---|---|---|---|
| 1 | 17.72 mΩ | 0.76 | 1.01 |
| 2 | 7.373 mΩ | 0.27 | 1.54 |
| 3 | 2.054 mF<br>686.8 m | 0.09<br>8.90 | 8.68<br>0.09 |
| 4 | 3.1 mΩ | 0.07 | 8.27 |
| 5 | 4.001 F<br>1 | 0.05 | 8.91 |
| 6 | 14.75 mΩ | 0.32 | 0.61 |
| 7 | 2.358 F<br>953.7 m | 0.17<br>25.46 | 2.75<br>0.01 |
| 8 | 1<br>12.38 mΩ<br>0 Ohm | 0.11 | 4.09 |
| 9 | 13.29 nH | 0.70 | 1.10 |
| modulus impedance error: mean 0.1 %, max. 0.8 %<br>phase angle error: mean 0.0 deg, max. 0.3 deg | | | |

Tab 3: Fit results of the system described in Fig.5

Fig 5: Nyquist and Bode plots of the impedance spectra for a SOFC at 850°C and at maximum load of 4.5A (≈ 0.3A/cm$^2$). The potential was -0.7V. Fuel gas: $H_2$ with 50% humidity, oxidant: air, 30 l/h both. Circles: measured data, lines: modeled curves. The EC is extended in the same way as in fig.3.

$$R_p(cathode) = \frac{\left[R_6 \cdot R_4\right]^{1/2}}{\tanh\left(\left[R_6 / R_4\right]^{1/2}\right)} \qquad (2)$$

and results in a value of 34.6 mΩ. This value can approximately be read directly from the real part of the Nyquist diagram. But this can only be done without resolution into the contributions R4 and R6, which are assigned to the integral oxygen exchange (transfer resistance) and the integral ionic conductivity. It must be stated, that the quality of the simulation in the frequency range from 5 to 50 Hz is inferior to the simulation in other frequency regions. According to [6], the reason is a diffusion hindrance of vapor in hydrogen in the gas channels in front of the porous anode system. In this frequency range it can be described as a RC combination. The results for the same measurement in view of this fact are shown in the figure 3. The simulation quality achieved with the applied models is excellent. Similar checks are necessary for the qualification of power-supplying cells with high current density. Higher currents are necessary, because the cathode shows significant activation on the load. Therefore one spectrum shows the impedance of a cell at its maximum allowable polarization, that means at a cell voltage of about -700 mV and a current of approximately 4.5 A.

The measurements have been carried out with a Zahner impedance measurement equipment (IM5d) in combination with an electronic load (EL 300). It is often necessary to make use of this load, because 30 A are reached with oxygen on the cathode and dry hydrogen on the anode and a geometric electrode area of 16 cm$^2$. This leads, however, to a limitation in the upper frequency range (< 10 KHz). The results shown in the figure 5 have been achieved under maximum load in air operation and by using a hydrogen-vapor mixture in a 1:1 ratio. This condition ensures a homogeneous current density distribution along the area of the anode and with this for the complete cell. This prerequisite together with a good linearity of the current/voltage characteristic of the cathode allowed to apply the model for homogeneous pore systems [3] not only at rest potential, but also under DC load. As is seen from the substitution of the parameter $R_6$ for the oxygen exchange, it is exactly this parameter value which is reduced by the DC current flow from 25.8 mΩ to 14.8 mΩ at the same temperature. The polarization resistance of the cathode therefore decreases too, according to (2). In summary, it can be stated that the application of impedance measurements are an approach to parameters, which have proved to be indispensable for development and quality control, especially at high currents in realistic cell setups. The following parameters are included:

- the series resistor as the sum of the bulk resistors of the installed layers
- the polarization resistances of the electrode, resolved into contributions for conductivity and exchange processes
- additional contributions of the gas supply hindrance near the electrode

The structure of the electrodes and the electrical contact between the layers could be optimized with the help of this information.

**References:**
[1] J. Winkler et al. "Geometric requirements to solid electrolyte cells with a reference electrode", to be published in the <International Electrochemical Society> Materials Department Riso, National Laboratory, DK-4000 Roskilde/Denmark
[2] K. Mund, Siemens research and development, Res. 4/2 (1975) 67
[3] H. Göhr et al. "Kinetic Properties of Smooth and Porous Lead/Lead Sulphate Electrodes", 34th ISE meeting, Erlangen 1983, poster 0715
[4] G. Paasch, P.H. Nguyen "Impedance of Inhomogeneous Porous Electrodes", this issue
[5] A. Hahn, Thesis, University Erlangen (1997/1998)
[6] J. Geyer et al. "Investigations into the Kinetics of the Ni-YSZ-Cermet Anode of a SOFC", Proc. of the 5th Internat. Symposium on SOFC, Proc. Vol. 97-40, <The Electrochemical Society> 1997

# *Impedance of Inhomogeneous Porous Electrodes*

## *A novel transfer matrix calculation method*

**by G. Paasch[1], P.H. Nguyen [1,2]**
[1] Institut für Festkörper- und Werkstofforschung, Universität Dresden, 01171 Dresden, Germany
[2] Physikalisches Institut und Bayreuther Institut für Makromolekülforschung (BIMF), Universität Bayreuth, 95440 Bayreuth, Germany

Transmission line models (TLM) [1] are widely used to describe the electrochemical impedance of porous electrodes or of solid oxide fuel cells. Contrary to a lot of real systems the distributed elements are supposed to be position independent (homogeneous system) in the usual TLM's. The authors developed a (4x4) transfer matrix calculation scheme for the impedance of an inhomogeneous TLM for two geometries, (a) the system metal/porous layer/electrolyte and (b) the system electrolyte/porous membrane/electrolyte. In this article the simplified (2x2) version (one resistivity negligible) for the geometry (a) and demonstrate examples for both geometries is presented.

### The transmission line model

Our treatment is based on the two-phase model described in [2-3]. In the electronic and ionic phases there are the potentials $\varphi_1$ and $\varphi_2$. On a length dx there are the resistivities $dRi = \rho_i\, dx / A$ ($i$ = 1 electronic, $i$ = 2 ionic) with the respective specific resistivities $\rho_i$ (which must account for the respective volume fractions of the phases). Both phases are continuously interconnected by a complex conductance $dG = gAdx$. This system can be represented by the TLM shown in Fig.1.

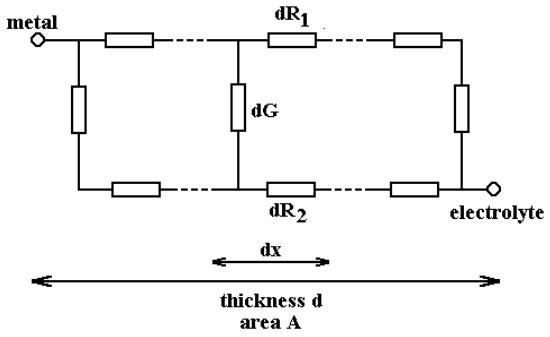


Fig.1: Transmission line model of porous electrode

The potential propagation is described (periodic time dependence with angular frequency $\omega$) by the two coupled differential equations.

$$g(\varphi_1-\varphi_2) = -\frac{d}{dx}\frac{1}{\rho_1}\frac{d\varphi_1}{dx}$$
$$-g(\varphi_1-\varphi_2) = -\frac{d}{dx}\frac{1}{\rho_2}\frac{d\varphi_2}{dx} \qquad (1)$$

where $g$, $\rho_1$, $\rho_2$ are in principle frequency dependent and position dependent. For a homogeneous system the potential propagation is determined by the complex decay length

$$\lambda = \left[g\left(\rho_1+\rho_2\right)\right]^{-\frac{1}{2}} \qquad (2)$$

Although the matrix method can be formulated for the general case we consider real resistivities here. As an example for the interconnection conductance we assume charge transfer (ct) as in [2-3] which is hindered in series by finite diffusion, both in parallel with double layer (dl) capacity (all at the pore surfaces). These processes are described by

$$g = CS\left(i\omega + \omega_0 Y\right) \qquad (3)$$
$$\omega_0 = \frac{j_0}{C}\frac{RT}{F} \qquad (4)$$

where $C$ is the dl capacity per unit area, $S$ is the pore area per unit volume, and the characteristic frequency $\omega_0$ contains the standard exchange current density $j_0$ of the ct process. The finite diffusion hindrance is contained in (3) by

$$Y = \left\{1 + \sqrt{\frac{\omega_2}{i\omega}} \coth \sqrt{\frac{i\omega}{\omega_3}}\right\}^{-1} \qquad (5)$$

$$\omega_2 = \tilde{k}^2 / D \qquad \omega_3 = D / l_p^2 \qquad (6)$$

where the two characteristic frequencies are determined by the (dominating) diffusion coefficient $D$, the reaction velocity $\tilde{k}$, and the characteristic length of the pores $\ell_p$ limiting the diffusion in the space. The complex decay length (2) is then specified as

$$\left(\frac{\lambda}{d}\right)^2 = \frac{\omega_1}{i\omega + \omega_0 Y} \qquad \omega_1 = \frac{1}{\boldsymbol{CS}(\rho_1 + \rho_2)\boldsymbol{d}^2} \qquad (7)$$

and for the assumed position independence of all parameters the impedance is for the geometry (a)

(layer covering a metal electrode) given by

$$\boldsymbol{Z}\frac{\boldsymbol{A}}{\boldsymbol{d}} = \frac{\rho_1^2 + \rho_2^2}{\rho_1 + \rho_2}\frac{\lambda}{\boldsymbol{d}}\coth\frac{\boldsymbol{d}}{\lambda} + \frac{2\rho_1\rho_2}{\rho_1 + \rho_2}\frac{1}{\sinh\frac{\lambda}{\boldsymbol{d}}} + \frac{\rho_1\rho_2}{\rho_1 + \rho_2} \qquad (8)$$

Applications and examples can be found in [2-5].

## The transfer matrix method

In the generally inhomogeneneous TLM the parameters depend on the coordinate perpendicular to the layer as demonstrated in Fig.2 for the resistivity $\rho(x)$ - in the following the simple case is considered that one resistivity is negligible $\rho_2 \equiv \rho(x) \gg \rho_1 \approx 0$. In order to describe this situation the layer is divided into $N$ slabs and in each slab each quantity is replaced by its mean value, e.g. $\rho_n = (\rho(x_{n-1}) + \rho(x_n)) / 2$. Then the potential propagation is determined by transfer matrices (such methods are common in other fields [6,7]) connecting the slabs $n$ and $n+1$.

$$\boldsymbol{M}_n = \frac{1}{2}\left[\begin{array}{c} (1+\boldsymbol{S}_n)\exp\left\{\chi_n\left(\frac{1}{\lambda_{n+1}} - \frac{1}{\lambda_n}\right)\right\}(1-\boldsymbol{S}_n)\exp\left\{-\chi_n\left(\frac{1}{\lambda_{n+1}} + \frac{1}{\lambda_n}\right)\right\} \\ (1-\boldsymbol{S}_n)\exp\left\{\chi_n\left(\frac{1}{\lambda_{n+1}} + \frac{1}{\lambda_n}\right)\right\}(1+\boldsymbol{S}_n)\exp\left\{-\chi_n\left(\frac{1}{\lambda_{n+1}} - \frac{1}{\lambda_n}\right)\right\} \end{array}\right] \quad \text{with} \quad \boldsymbol{S_n} = \frac{\lambda_n \rho_n}{\lambda_{n+1}\rho_{n+1}} \qquad (9)$$

The potential propagation through the whole layer is determined by the matrix product

$$M = \prod_{n=1}^{N} M_n \qquad (10)$$

For the geometry (a) (Fig.2) the appropriate boundary conditions lead to the impedance

$$\boldsymbol{Z}\frac{\boldsymbol{A}}{\boldsymbol{d}} = -\rho(0)\frac{\lambda_1}{\boldsymbol{d}}\frac{(\boldsymbol{M}_{11} + \boldsymbol{M}_{21})e^{-2d/\lambda_N} + (\boldsymbol{M}_{12} + \boldsymbol{M}_{22})}{(\boldsymbol{M}_{11} - \boldsymbol{M}_{21})e^{-2d/\lambda_N} + (\boldsymbol{M}_{12} - \boldsymbol{M}_{22})} \qquad (11)$$

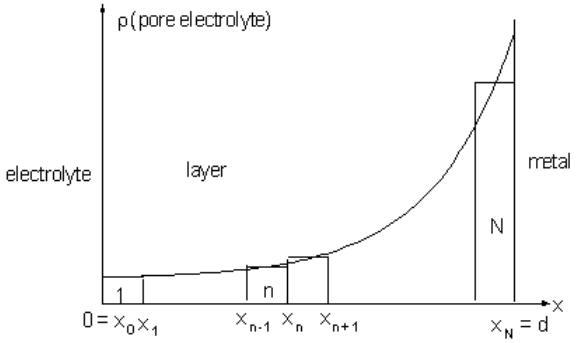


Fig.2: Position dependence of the resistivity and splitting the layer into N slabs.

Here, $M_{ij}$ are the four elements of the matrix $M$ (10). For a homogeneous system it is seen from (9), (10) that $M_{11} = M_{22} = 1$ and $M_{12} = M_{21} = 0$ and (11) is reduced to (8) (with $\rho_1 = 0$ as assumed here and $\rho_2 = \rho(0)$). With (9) to (11) a fast and simple calculation of the impedance is possible for arbitrarily chosen position dependencies of the parameters of the system. The number $N$ of the slabs depends on the position dependence one wants to describe. For the membrane geometry (b) there are only other boundary conditions than for (11) but the impedance is determined by the same matrix $M$.

## Examples

In the following it is demonstrated that position dependent parameters of TLM's can cause significant qualitative modifications of the impedance. A position dependence of the resistivity is considered for simplicity only. This is shown in Fig.2. The dependence

$$\rho(\boldsymbol{x}) = \rho_0\left(1 + \frac{\Delta\rho}{\rho_0}\exp\left\{\frac{\boldsymbol{d}}{\boldsymbol{L}}\left(\frac{\boldsymbol{x}}{\boldsymbol{d}} - 1\right)\right\}\right) \qquad (12)$$

is used to describe an increase of the resistivity towards one side (for the layer coating a metal towards the interface with the metal). This simple dependence contains as parameters only the maximum increase $\Delta\rho / \rho_0$ and a characteristic length $L$. For $d/L \gg 1$ the resistivity increases from $\rho_0$ to $\rho_0 + \Delta\rho$ in the immediate neighborhood of the interface only, whereas for $d/L \ll 1$ the resistivity is almost constant $\rho_0 + \Delta\rho_0$. In the examples only one value $\Delta\rho / \rho_0 = 10$ has been chosen but different values $d/L$ (0.1, 1, 10). As just explained, the most interesting case will be a value near $d/L = 1$. For the three val-

ues *d/L* the number *N* which almost gives the exact results are about 20, 80, 120. The four characteristic frequencies (4), (6) and (7) have for $\rho_0$ the values $\omega_0$ = 100s$^{-1}$ $\omega_1$ = 10s$^{-1}$ $\omega_2$ = 0.1s$^{-1}$ $\omega^3$ = 0.001s$^{-1}$. The impedance is shown in the figures in the Nyquist representation and for better orientation 4 fixed frequencies ($\omega$ / 2 $\pi$ = 10$^3$, 10, 0.1, 0.001 Hz) are denoted by symbols (o etc.) from left to right. Fig.3 shows the impedance for the layer coating a metal electrode and Fig.4 shows the results for a membrane for the same parameters.

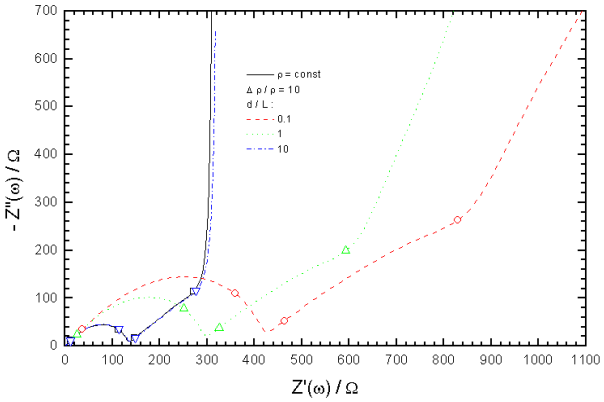


Fig.3: Impedance of a porous layer covering a metal. Parameters explained in the text.

For a constant resistivity $\rho_0$ due to the choice of the characteristic, frequencies in both cases for high frequencies, a depressed and right scewed arc, are arising from the distributed ct and dl elements. This part is clearly separated from the low frequency behavior determined by the finite diffusion in the pores. For the layer this leads to the Warburg

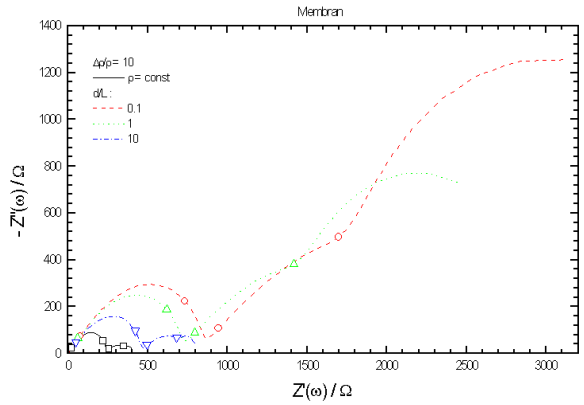


Fig.4: Impedance of a porous membrane.

behavior and to a capacitive behavior for even smaller frequencies. In the case of membrane both is compressed in the smaller arc as a result of the modified boundary conditions. Inclusion of the position dependence (12) of the resistivity leads not only to a general scaling to higher impedances but modifies the low frequency behavior qualitatively in particular. For the layer the most striking change is the transformation of the capacitive low frequency behavior into a CPE-like behavior (in the same frequency range). For the membrane on the other hand the two different diffusion parts become separated from each other and apparently one has a superposition of three arcs. Finally, Fig.5 shows for *d/L* = 10 the case of a layer when the resistivity of the pore electrolyte increases either towards the

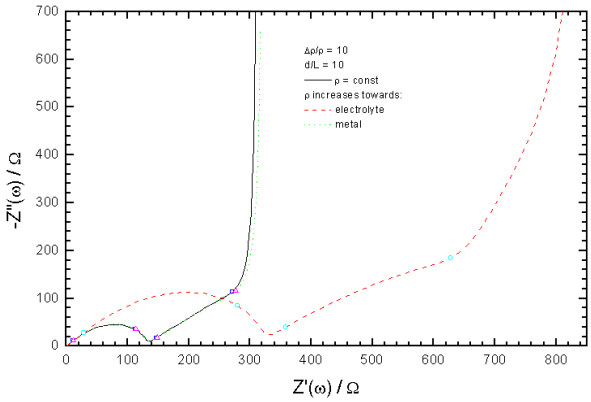


Fig.5: As Fig.4 but increase of $\rho$ towards the metal (---) and towards the electrolyte (…)

interface with the metal or towards the electrolyte. The qualitative difference between both cases can be understood as follows. In the first case, the small metal-near region with high resistivity results effectively in a "thinner" layer. But in the second case, the potential can penetrate into the layer through the thin high resistive region only.

## Conclusion

The examples show clearly the importance to consider thoroughly parameter dependencies of inhomogeneous TLM's to avoid serious misinterpretations of measured impedances. The method sketched here shortly provides a fast and simple tool for the calculation of the electrochemical impedance of inhomogeneous TLM's. The more general (4x4) version of the method will be published . It should be noted that the matrix method given in [8] does not solve the boundary value problem explicitly.

## References

[1] J. R. Macdonald, *Impedance Spectroscopy*. Wiley, New York (1987)
[2] G. Paasch, K. Micka, P. Gersdorf, Electrochim. Acta **38** (1993) 2653
[3] G. Paasch, S. Ludwig, K. Micka, in W. Schmickler (Ed.) *Ladungsspeicherung in der Doppelschicht*, Ulmer Universitätsverlag, 1995 p.151-175
[4] K. Roßberg, G. Paasch, S. Ludwig, L. Dunsch, to be published
[5] G. Paasch, C. Ehrenbeck, K. Jüttner, to be published
[6] J. Lekner, Theory of Reflection, Martinus Nijhoff Publ., Dordrecht / Boston / Lancaster, 1987
[7] P. H. Nguyen, G. Paasch, G. Gobsch, 35. Int. Wiss. Koll. TH Ilmelnau,Heft 4 (1990) p.21, P. H. Nguyen, Dissertation, TH Ilmelnau, 1990.
[8] K. Eloot, F. Debuyck, M. Moors, A. P. van Peteghem, J. Appl.Electrochem. **25** (1995) 326, 334

# *Main error sources at AC measurements on low impedance objects*

**by C.A. Schiller**
Zahner-elektrik GmbH & Co. KG

At a first glance, AC impedance measurements seem to be a simple task: As in DC measurement setups one has to compare a response signal coming from an examined object (current or potential resp.) with a stimulation signal applied to the object (potential or current resp.). The difference is to use AC instead of DC signals.

Since almost perfect equipment exists, measurement accuracy problems are more problems of the expectations of the user and less problems of the instrumentation itself: Even very experienced scientists in the fields of EIS can hardly estimate the significance of parasitic effects when moving from lower to higher frequencies. Origin and phenomenology of artifacts as well as remedies for them differ totally, if one measures very low or very high impedances. Although high impedance artifacts are very important for wide fields of EIS, in accordance with the focus of this issue of **EIApps**, only low impedance effects shall be treated here. Additional artifacts will be treated in the next issues.

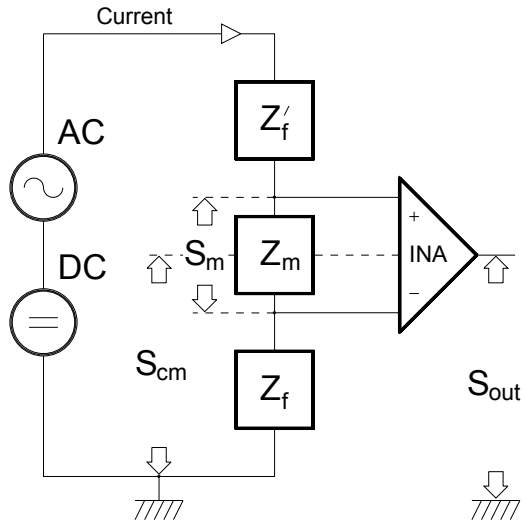


Fig.1: Common mode effects in an impedance measurement arrangement.

The main error sources for low impedance objects arise from the competition between the small impedance of the object and the comparable or even much higher series impedances of the feed wires. Two different kinds of interference are important here: Common mode interference and coupling interference. The first one results from overstressing a specific ability of the instruments input amplifiers and is called *common mode rejection ratio* (**CMMR**). Every instrumentation amplifier has not only a well defined and wanted sensitivity for signals as a difference between its input terminals. In addition a small, but unwanted sensitivity exists for "common mode signals", which are defined as signals fed to both amp inputs in parallel and referred to ground. The **CMMR** is the quotient between the wanted differential- and the unwanted common mode sensitivity. Fig. 1 shows the appearance of common mode effects in a simplified impedance measurement arrangement. The *signal- to common mode ratio* **SCMR** (equ. 1) defines the suppression of unwanted contributions from common mode effects.

$$SCMR = CMMR * S_m / S_{cm} \;;\; S_m / S_{cm} = Z_m / Z_f \quad (1)$$

An example shall illustrate the effect. A fuel cell electrode has an impedance of about 100 mΩ at DC. One meter of a typical labor cable used as a feed wire has a series resistance in the same order of magnitude. The **SCMR** is near the **CMMR**, which is typically in the range of $10^5$ for a DC amplifier. This error contribution at DC in the range of $10^{-5}$ is negligible. But at 100 KHz the cell impedance is reduced to about 10 mΩ, while the series impedance modulus of the feed wire is increased to about 1 Ω caused by its inductivity. In addition the CMMR of instrumentation amplifiers is much less at high frequencies than at DC. For instance the popular *INA* series of Burr Brown show a **CMMR** of $10^5$ at DC but only 10 to 100 at 100 KHz. This leads to a SCMR of only 1 for typical amplifiers on the market and about 300 in the case of the IM6 with its much better initial **CMMR**. In case of the IM6 the *common mode error contribution* would cause a deviation in the phase angle of about 2 degrees and 0.3 % in the impedance modulus. Short and thick lead wires can help to minimize such errors.

The second type of low impedance errors is caused by coupling effects between current-feeding and potential-sensing lines. It diminishes at DC, but becomes dramatic at higher frequencies. Even the best amplifier technique cannot suppress this effect, because it affects the measurands themselves. The origin is the so called *mutual inductance* between the above mentioned lines, which may be understood as a transformer arrangement (fig. 2). If one would lead current feed and potential sense cables side by side and in parallel, the error effect would be at its maximum. All magnetic field of the current path would be common with the potential sensing path. Under such worst case conditions 0.3 % uncertainty in the impedance modulus can be reached already at 30 Hz! Because magnitude and sign of the contaminating signals are varying with

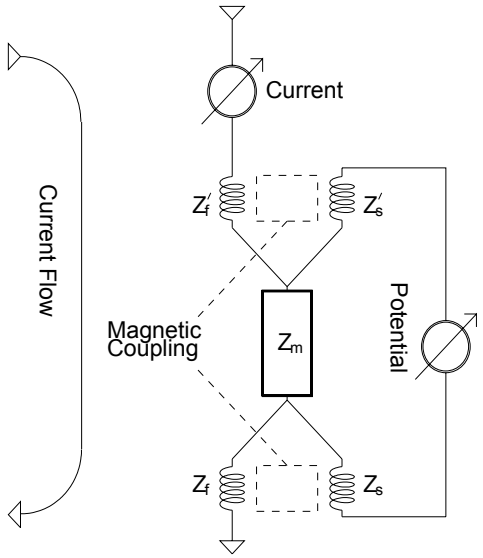


Fig.2: *Mutual inductance* may be understood as a transformer arrangement.

the geometry, the phase angle may be shifted between inductive, capacitive and almost zero error, while the impedance modulus is heavily distorted even at correct phase angle. Cable shielding does not help. The only way to suppress the *mutual inductance errors* as far as possible, is to minimize the magnetic coupling. In practice one should use one twisted pair for the current feeding lines and a second one for the potential sensing lines. So the magnetic field of the current, flowing to the object, is almost perfectly compensated by the inverse field of the current flowing back. The small residual field will influence the sense line of normal and that one of the inverse polarity in the same way. This will create only common mode signal, which may be suppressed by a good instrumentation (Fig. 3).

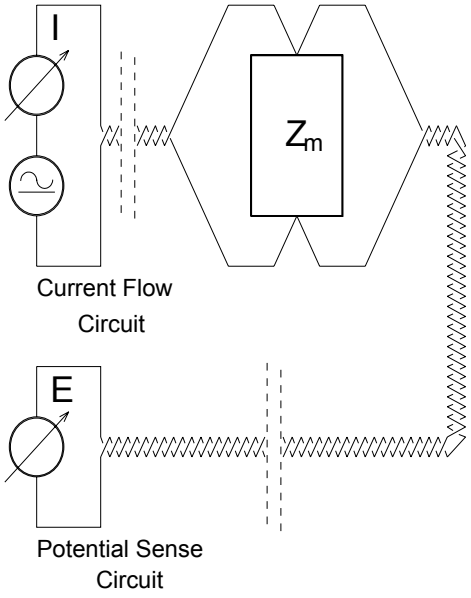


Fig.3: Twisted pairs of current feeding and potential sensing lines suppress the *mutual inductance errors*.

What we can learn is, that the best wiring and the best instrumentation is not able to suppress the *mutual inductance error* completely, because of the finite dimensions of the examined object itself. A rule of thumb may help not to overstress the expectations on the significance of low-impedance-high-frequency measurements. The maximum frequency, which makes sense to investigate, is given by equation 2:

$$f_{max} = 1\ \text{MHz} / Z_m \qquad (2)$$

This limit can only be reached or slightly exceeded by a careful wiring.

# *FAQs*

***How can I reduce the measuring time for my impedance spectra?***

A reduction of the measuring time will often be demanded in case of examining non steady state systems or in case of using very low frequency ranges down to mHz or μHz. At low frequencies polychromatic stimulation (PS) at first glance promises advantages in comparison to monochromatic (MS) experiments. By a rough estimation the measuring time of PS methods is fixed by the sum of all periods $n_e$ at the lowest frequency which is investigated, namely the $\omega_0$ fundamental.

$$T_{tot,\,poly} = \frac{n_e \cdot 2\pi}{\omega_0} = \frac{n_e}{f_0} = n_e \cdot T_0$$

In contrast the minimum measuring time of MS (sine wave) experiments is given by the sum of periods $n_{e,i}$ of all frequencies $\omega_i$ to be measured.

$$T_{tot,\,mono} = \sum_{\omega 0}^{\omega\,\max} \frac{n_{e,i} \cdot 2\pi}{\omega_i} = \sum_{k=1}^{k\,\max} \frac{n_{e,i}}{k \cdot f_0} \approx n_e \cdot T_0 \cdot \sum_{k=1}^{k\,\max} \frac{1}{k} = n_e \cdot T_0 \cdot f_{res}$$

A comparison of typical measuring times for both methods is quite difficult as there are some unknown scaling factors. Under the assumption of an ideal measuring object where no ranging processes will occur the scaling factor $f_{res}$ in first order depends on the number of measuring points of the lowest decade.

| # points | 2 | 3 | 4 | 5 | 6 | 7 | 8 | 9 | 10 |
|---|---|---|---|---|---|---|---|---|---|
| $f_{res}$ | 1.32 | 1.68 | 2.06 | 2.44 | 2.82 | 3.21 | 3.60 | 3.99 | 4.38 |

The ratio of e.g. $\frac{T_{mono,5}}{T_{poly}} = \frac{2.44}{1} = 2.44$

This shows a slight advantage for PS. If, however, at least one ranging process is necessary during measurement, this factor will be reduced to about 1.3. In PS methods ranging processes dominate the measuring time (T,2T, 3T,etc), while MS can use dynamic ranging. Then the measuring time is extended only by a factor of 1/n, depending on the measuring frequency $n\omega_0$. One sees, that the simple speculation to save time will not work very good, even neglecting all aspects of accuracy. But in addition, using PS the total energy of the signal will be spread over all examined frequencies. Only the average fraction $E_f \approx E/n$, compared with the monochromatic case will be available for one frequency line. To avoid nonlinear response the AC amplitude has to be selected sufficiently low. Thus polychromatic stimulation has to be repeated n-fold to obtain sufficient signal to noise ratio. This leads to significant longer measuring times than in the case of single sine methods which contradicts the expectations of the user. This fact has been proved by Miloco in 1994 [1]

Nevertheless, regarding non steady state system research, there is a gap, where PS shows clear advantage. In the higher frequency range (>100 Hz) the pure measuring time will no longer dominate the overall time. Most of it is spent by the instruments microprocessor system analyzing the incoming data after each frequency sample. In the PS case, the sum of all this analysis time appears at the end of a measurement, the measurement itself is much faster. This is an advantage when studying non steady state systems. For this application the PS method was developed further by Schindler and Popkirov [2]. A version of PS can be performed with the IM6, extended by the TR8M transient recorder module.

It must be mentioned, that regarding non steady state behavior, there are several possibilities to increase the reliability of the AC impedance results, if measurement time reduction is impossible:
a) IM6 on-line drift correction: Periodic stimulation offers the detection of non steady state behavior of the investigated system. The IM6 performs an automatic drift correction in the lower frequency mode.
b) LKKT (Logarithmic Kramers Kronig Transform): By means of the LKKT [3] not only violations of the EIS fundamentals of the examined system may be detected. The LKKT version in the THALES analysis software allows the reconstruction of non-affected spectra, if the violations are not too strong.
c) Interpolation of impedance spectra series versus time: Series measurements vs. time offer a further possibility to correct impedance spectra of drifting systems. Under the assumption of slow rates of changes the data may be corrected. The spectra can be transformed by an interpolation routine generating new ones, belonging to unique times. Finally each of those spectra will represent a certain state of the electrode. [4,5] This method is also available in the THALES-software package. (BR)

[1] Ruben H. Milocco: Minimal measurement time in electrochemical impedance identification. Electrochimica acta, Vol.39, No.10, pp 1433-1439, 1994
[2] G.S. Popkirov and R.N. Schindler: A new impedance spectrometer for the investigation of electrochemical systems. Rev. Sci. Instrum. 63 (11), 1992
[3] H. Göhr, B. Röseler and C.A. Schiller: Advantages of Hilbert Transform compared with Kramers-Kronig Rule when examining the causality of electrochemical impedance spectra. Presented at the 46th ISE Meeting, Xiamen, China, 1995
[4] Z. Stoynov: Nonstationary impedance spectroscopy. Electrochem. Acta 38, no. 14, pp. 1919-1922 (1993)
[5] H. Göhr, H. Bode, A. Burghart and C.A. Schiller: Impedance measurements at electrodes of continuously changing state. Presented at the 2nd EIS Symposium, Santa Barbara, USA, 1992

**Editorial**
***Electrochemical Applications*** is published by
***Zahner-elektrik*** GmbH & Co. KG
Thüringer Str. 12, D-96317 Kronach, Germany
Tel.: 09261-52005 / Fax: -51919 / BBS: -52004
email: zahner@aol.com
**Editors**: Dr. Hans-Joachim Schäfer (Zahner-elektrik), Carl Albrecht Schiller (Zahner-elektrik)

**Authors of this issue**: Prof. Dr. Hermann Göhr (Erlangen), Dr. P.H. Nguyen (Universität Bayreuth), Prof. Dr. G. Paasch (Institut für Festkörper- und Werkstofforschung, Dresden), Dr. Franz Richter (Siemens AG, Erlangen), Dr. Burkhard Röseler (BR, Zahner-elektrik), Carl Albrecht Schiller (CAS, Zahner-elektrik)